

Journal of Coordination Chemistry

Publication details, including instructions for authors and subscription information:

<http://www.tandfonline.com/loi/gcoo20>

Crystal structures and DNA-binding properties of Pr^{III} complexes derived from 8-hydroxyquinoline-2-carboxaldehyde and three arylhydrazines

Yong-Chun Liu^a, Ying-Ying Li^a, Hui-Li Qi^a, Ke-Jun Zhang^a, Rui-Xia Lei^a & Jian-Ning Liu^a

^a College of Chemistry and Chemical Engineering, Longdong University & FLUOBON Surfactant Engineering Technology Center, Longdong University, Qingyang, PR China

Accepted author version posted online: 03 Oct 2014. Published online: 30 Oct 2014.



CrossMark

[Click for updates](#)

To cite this article: Yong-Chun Liu, Ying-Ying Li, Hui-Li Qi, Ke-Jun Zhang, Rui-Xia Lei & Jian-Ning Liu (2014) Crystal structures and DNA-binding properties of Pr^{III} complexes derived from 8-hydroxyquinoline-2-carboxaldehyde and three arylhydrazines, *Journal of Coordination Chemistry*, 67:22, 3689-3703, DOI: [10.1080/00958972.2014.972387](https://doi.org/10.1080/00958972.2014.972387)

To link to this article: <http://dx.doi.org/10.1080/00958972.2014.972387>

PLEASE SCROLL DOWN FOR ARTICLE

Taylor & Francis makes every effort to ensure the accuracy of all the information (the "Content") contained in the publications on our platform. However, Taylor & Francis, our agents, and our licensors make no representations or warranties whatsoever as to the accuracy, completeness, or suitability for any purpose of the Content. Any opinions and views expressed in this publication are the opinions and views of the authors, and are not the views of or endorsed by Taylor & Francis. The accuracy of the Content should not be relied upon and should be independently verified with primary sources of information. Taylor and Francis shall not be liable for any losses, actions, claims, proceedings, demands, costs, expenses, damages, and other liabilities whatsoever or howsoever caused arising directly or indirectly in connection with, in relation to or arising out of the use of the Content.

This article may be used for research, teaching, and private study purposes. Any substantial or systematic reproduction, redistribution, reselling, loan, sub-licensing,

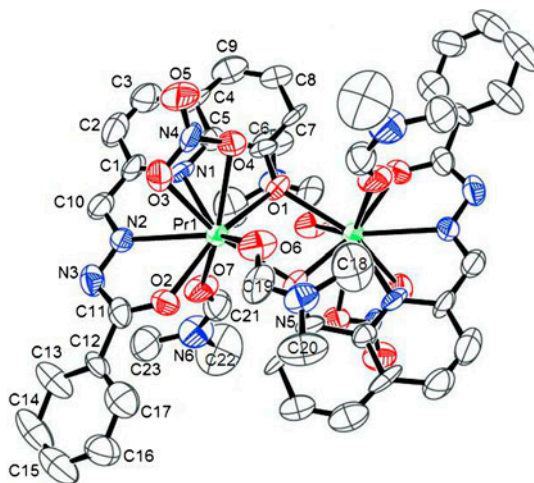
systematic supply, or distribution in any form to anyone is expressly forbidden. Terms & Conditions of access and use can be found at <http://www.tandfonline.com/page/terms-and-conditions>

Crystal structures and DNA-binding properties of Pr^{III} complexes derived from 8-hydroxyquinoline-2-carboxaldehyde and three aroylhydrazines

YONG-CHUN LIU*, YING-YING LI, HUI-LI QI, KE-JUN ZHANG, RUI-XIA LEI and JIAN-NING LIU

College of Chemistry and Chemical Engineering, Longdong University & FLUOBON Surfactant Engineering Technology Center, Longdong University, Qingyang, PR China

(Received 1 April 2014; accepted 10 September 2014)



Pr^{III} and three synthesized ligands, 8-hydroxyquinoline-2-carboxaldehyde-(benzoyl)hydrazone, 8-hydroxyquinoline-2-carboxaldehyde-(2'-hydroxybenzoyl)hydrazone, and 8-hydroxyquinoline-2-carboxaldehyde-(isonicotinyl)hydrazone, respectively, can form binuclear Pr^{III} complexes with 1 : 1 metal-to-ligand stoichiometry and nine-coordination at Pr^{III} indicated by X-ray crystal structural analyses. Ligands are dibasic tetradentate, binding to Pr^{III} through the phenolate oxygen, nitrogen of quinolinato unit, the C=N of methylene, and ⁻O=C=N- enolized and deprotonated from O=C-NH- of the aroylhydrazone side chain. One DMF binds orthogonally to the ligand plane from one side to the metal ion, while another DMF and a bidentate nitrate simultaneously bind from the other. Dimerization of the monomeric unit occurs through the phenolate oxygen leading to a central planar four-membered (PrO)₂ ring. The crystal structures are similar to each other and to other nine-coordinate lanthanide complexes with geometry of distorted edge-sharing mono-capped square-antiprism of [LnL(NO₃)(DMF)₂]₂ (Ln = La^{III}, Nd^{III}, Sm^{III}, Eu^{III}, Tb^{III}, Dy^{III}, Ho^{III}, and Er^{III}) except for Yb^{III} with eight-coordinate Yb^{III} center with distorted edge-sharing dodecahedron of [YbL(NO₃)(DMF)₂]₂.

*Corresponding author. Email: ychliu001@163.com

derived from 8-hydroxyquinoline-2-carboxaldehyde and aroylhydrazines. The ligands and Pr^{III} complexes can bind to calf thymus DNA through intercalation with binding constants at 10^5 M^{-1} and probably be used as potential antitumor drugs.

Keywords: Rare earth metal; Praseodymium complex; X-ray crystallography; Calf thymus DNA; Intercalation

1. Introduction

A number of metal chelates, as agents for mediation of strand scission of duplex DNA and as chemotherapeutic agents, have been used as probes of DNA structure in solution [1–3]. Apart from magnetic and photophysical properties, the bioactivities of lanthanide complexes such as antimicrobial, antitumor, antiviral, anticoagulant action, enhancing NK and Macrophage cell activities, prevention from arteriosclerosis, etc have been explored [4–7]. Schiff bases are able to inhibit the growth of several animal tumors, and some metal chelates have shown good antitumor activities against animal tumors [8, 9]. Well-designed organic ligands can have special properties fine tuned by metal ions. The chemistry of quinoline and its derivatives has also attracted special interest due to their therapeutic properties. Quinoline sulphonamides have been used in the treatment of cancer, tuberculosis, diabetes, malaria, and convulsions [10, 11]. Previously, a series of lanthanide complexes were prepared from lanthanide metal ions with 8-hydroxyquinoline-2-carboxaldehyde-aroylhydrazones and 8-hydroxyquinoline-7-carboxaldehyde-aroylhydrazones [12–21]. These lanthanide complexes have similar structures and present strong affinities of binding to DNA through intercalation. In this study, three Pr^{III} complexes prepared from 8-hydroxyquinoline-2-carboxaldehyde with aroylhydrazines and their crystal structures and DNA-binding properties will be addressed.

2. Experimental

2.1. Materials

Calf thymus DNA (CT-DNA) and ethidium bromide (EB) were obtained from Sigma-Aldrich Biotech. Co., Ltd. The stock solution (1.0 mM) of the investigated compound was prepared by dissolving the powdered material into appropriate amounts of DMF solution. Deionized double distilled water and analytical grade reagents were used throughout. CT-DNA stock solution was prepared by dissolving the solid material in 5 mM Tris–HCl buffer (pH 7.20) containing 50 mM NaCl. The CT-DNA concentration in terms of base pair L^{-1} was determined spectrophotometrically by employing an extinction coefficient of $\varepsilon = 13,200 \text{ M}^{-1} \text{ cm}^{-1} (\text{base pair})^{-1}$ at 260 nm, and the concentration in terms of nucleotide L^{-1} was also determined spectrophotometrically by employing an extinction coefficient of $6600 \text{ M}^{-1} \text{ cm}^{-1} (\text{nucleotide})^{-1}$ at 260 nm [22]. The stock solution was stored at $-20 \text{ }^\circ\text{C}$ until it was used. EB was dissolved in 5 mM Tris–HCl buffer (pH 7.20) containing 50 mM NaCl and its concentration was determined assuming a molar extinction coefficient of $5600 \text{ M}^{-1} \text{ cm}^{-1}$ at 480 nm [23].

2.2. Methods

The melting points of the compounds were determined on an XT4-100X microscopic melting point apparatus (Beijing). The IR spectra were recorded on a Nicolet Nexus 670 FT-IR spectrometer using KBr disks from 4000 to 400 cm^{-1} . ^1H NMR spectra were recorded on a Bruker Advance DRX 200-MHz spectrometer with tetramethylsilane as an internal standard.

Viscosity titration experiments were carried out on an Ubbelohde viscometer in a thermostated water bath maintained at 25.00 ± 0.01 °C. Data were presented as $(\eta/\eta_0)^{1/3}$ versus the ratio of the compound to DNA, where η is the viscosity of DNA in the presence of the compound corrected from the solvent effect and η_0 is the viscosity of DNA alone [23, 24].

Ultraviolet–visible (UV–vis) spectra were obtained using a Specord 50 (Analytik Jena) UV–vis spectrophotometer with a 1 cm quartz cell. The binding constant (K_b) was determined by the following equation [25, 26]:

$$\frac{[\text{DNA}]}{\varepsilon_f - \varepsilon_a} = \frac{[\text{DNA}]}{\varepsilon_f - \varepsilon_b} + \frac{1}{K_b(\varepsilon_f - \varepsilon_b)} \quad (1)$$

where $[\text{DNA}]$ is the molar concentration of DNA in base pairs, ε_a ($\text{M}^{-1} \text{cm}^{-1}$) corresponds to the extinction coefficient observed, ε_f ($\text{M}^{-1} \text{cm}^{-1}$) corresponds to the extinction coefficient of the free compound, ε_b ($\text{M}^{-1} \text{cm}^{-1}$) is the extinction coefficient of the compound when fully bound to DNA, and K_b is the intrinsic binding constant. The ratio of slope to intercept in the plot of $[\text{DNA}]/(\varepsilon_f - \varepsilon_a)$ versus $[\text{DNA}]$ gives the values of K_b .

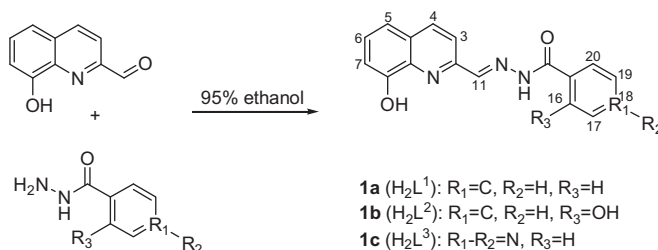
Fluorescence spectra were recorded using a RF-7000 spectrofluorophotometer (Hitachi) with a 1 cm quartz cell. The excitation and emission band widths were 10 nm. DNA-EB quenching assay was performed according to the literature procedure [12–21]. DNA (4.0 μM , nucleotides) solution was added incrementally to 0.32 μM EB solution, and then small aliquots of concentrated solutions (1.0 mM) were added till the drop in fluorescence intensity ($\lambda_{\text{ex}} = 525$ nm, $\lambda_{\text{em}} = 587$ nm) reached a constant value. Measurements were made after 5 min at 298 K. Stern–Volmer equation was used to determine the fluorescence quenching mechanism [27]:

$$F_0/F = 1 + K_{\text{SV}}[Q] \quad (2)$$

where F_0 and F are the fluorescence intensities in the absence and in the presence of a compound at $[Q]$ concentration, respectively; K_{SV} is the Stern–Volmer dynamic quenching constant.

2.3. Preparation of ligands (1a, 1b, and 1c)

The synthetic routes for **1a–c** are presented in figure 1 [12–19]. Ligand **1a**, 8-hydroxyquinoline-2-carboxaldehyde-(benzoyl)hydrazone, was prepared by refluxing and stirring a 10 mL ethanol solution of 8-hydroxyquinoline-2-carboxaldehyde (0.519 g, 3 mM) and a 10 mL 90% ethanol aqueous solution of benzoylhydrazine (0.408 g, 3 mM) for 8 h. After cooling to room temperature, the precipitate was filtered, recrystallized from 80% methanol aqueous solution, and dried in vacuum for 48 h to give a powder. Yield: 0.656 g, 74.7%. Pale. M.p. 221 °C (d). IR (KBr) ($\nu_{\text{max}}/\text{cm}^{-1}$): 3359 (NH), 3318 (OH), 1682 (C=O), 1602 (C=N, azomethine), 1546 (C=N, pyridine), 1267 (C–OH). UV–vis (λ_{max} nm, $\varepsilon \times 10^4 \text{M}^{-1} \text{cm}^{-1}$, DMF): 295, 3.55; 323, 2.11. NMR (^1H DMSO- d_6 (dimethyl sulfoxide

Figure 1. Synthetic routes for **1a-c**.

with both methyl groups deuterated), 200 MHz, ppm, s: singlet, d: doublet, t: triplet, m: multiplet): 8.637 (1H, s, 11- $CH=N$), 8.343 (1H, d, 4- CH , $^3J_{HH} = 8.8$ Hz), 8.119 (1H, d, 3- CH , $^3J_{HH} = 8.8$ Hz), 7.936 (2H, d, 16,20- CH , $^3J_{HH} = 6.4$ Hz), 7.630–7.507 (3H, m, 17,18,19- CH), 7.467–7.387 (2H, m, 5,6- CH), 7.131 (1H, d, 7- CH , $^3J_{HH} = 5.0$ Hz).

8-Hydroxyquinoline-2-carboxaldehyde-(2'-hydroxybenzoyl)hydrazone (**1b**) was obtained from equimolar amounts of 8-hydroxyquinoline-2-carboxaldehyde and 2-hydroxybenzoylhydrazine in the same way as **1a**. Yield: 0.746 g, 81.0%. Yellow. M.p. 245–247 °C (d). IR (KBr) (ν_{max}/cm^{-1}): 3464 (NH), 3250 (OH), 1643 (C=O), 1607 (C=N, azomethine), 1532 (C=N, pyridine), 1288 (C–OH). UV–vis (λ_{max} nm, $\epsilon \times 10^4 M^{-1} cm^{-1}$, DMF): 294, 3.16; 329, 2.36. NMR (1H DMSO- d_6 , 200 MHz, ppm): 8.621 (1H, s, 11- $CH=N$), 8.356 (1H, d, 4- CH , $^3J_{HH} = 8.6$ Hz), 8.113 (1H, d, 3- CH , $^3J_{HH} = 8.6$ Hz), 7.871 (1H, d, 20- CH , $^3J_{HH} = 7.8$ Hz), 7.469–7.395 (3H, m, 5,6,18- CH), 7.133 (1H, d, 7- CH , $J = 7.0$ Hz), 7.018–6.943 (2H, m, 17,19- CH).

8-Hydroxyquinoline-2-carboxaldehyde-(isonicotinyl)hydrazone (**1c**) was also obtained from equimolar amounts of 8-hydroxyquinoline-2-carboxaldehyde and isonicotinylhydrazine in the same way as **1a**. Yield: 0.622 g, 71.0%. Yellow. M.p. 162–164 °C (d). IR (KBr) (ν_{max}/cm^{-1}): 3576 (NH), 3193 (OH), 1663 (C=O), 1613 (C=N, azomethine), 1557 (C=N, pyridine), 1271 (C–OH). UV–vis (λ_{max} nm, $\epsilon \times 10^4 M^{-1} cm^{-1}$, DMF): 290; 2.86; 325, 1.78. NMR (1H DMSO- d_6 , 200 MHz, ppm): 8.813 (2H, d, 17,19- CH , $^3J_{HH} = 5.2$ Hz), 8.657 (1H, s, 11- $CH=N$), 8.372 (1H, d, 4- CH , $^3J_{HH} = 8.8$ Hz), 8.129 (1H, d, 3- CH , $^3J_{HH} = 8.8$ Hz), 7.861 (2H, d, 16,20- CH , $^3J_{HH} = 5.2$ Hz), 7.528–7.409 (2H, m, 5,6- CH), 7.148 (1H, d, 7- CH , $^3J_{HH} = 6.4$ Hz).

2.4. Preparation of the Pr^{III} complexes (**2a**, **2b**, and **2c**)

Complex **2a** was prepared by refluxing and stirring equimolar amounts of $Pr(NO_3)_3 \cdot 6H_2O$ and a 40 mL methanol solution of **1a** (0.0582 g, 0.2 mM) on a water bath. After refluxing for 30 min, triethylamine (0.020 g, 0.2 mM) was added into the reaction mixture dropwise to deprotonate the phenolic hydroxyl substituent of 8-hydroxyquinolinate. Then, the mixture was refluxed and stirred continuously for 8 h. After cooling to room temperature, the precipitate was centrifuged, washed adequately with hot methanol, and dried in vacuum over 48 h to give a powder. Yield: 0.090 g, 70.5%. IR (KBr) (ν_{max}/cm^{-1}): 3439 (OH, H_2O), 1591 (C=N, azomethine), 1544 (C=N, pyridine), 1493 (ν_1), 1331 (ν_4), 1102 (C–OM), 1058 (ν_2), 933 (ρ_τ), 838 (ν_3), 737 (ν_5), 690 (ρ_w), 561 (MO), 487 (MN), $\nu_1 - \nu_4 = 162$. UV–vis (λ_{max} nm, $\epsilon \times 10^4 M^{-1} cm^{-1}$, DMF): 321, 4.83; 368, 2.76.

Complex **2b** was prepared from equimolar amounts of $Pr(NO_3)_3 \cdot 6H_2O$ with **1b** (0.0614 g, 0.2 mM) as for **2a**. Yield: 0.093 g, 67.3%. IR (KBr) (ν_{max}/cm^{-1}): 3441 (OH,

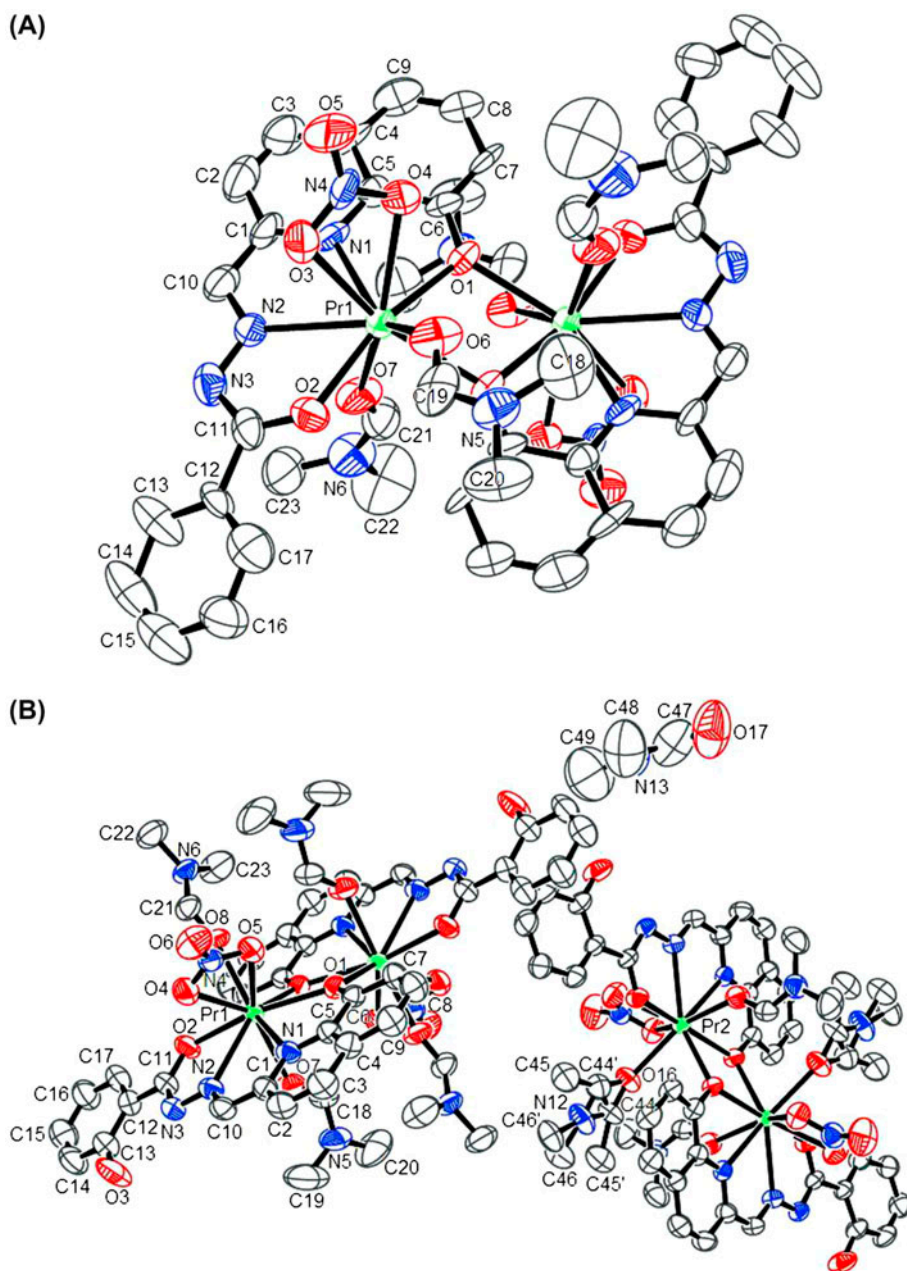


Figure 2. The structures of $[\text{PrL}^{1a}(\text{NO}_3)(\text{DMF})_2]_2$ (A), $[\text{PrL}^{1b}(\text{NO}_3)(\text{DMF})_2] \cdot \text{DMF}$ (B), and $[\text{PrL}^{1c}(\text{NO}_3)(\text{DMF})_2]_2$ (C).

H_2O), 3188 (OH, phenolic), 1604 (C=N, azomethine), 1587 (C=N, pyridine), 1489 (ν_1), 1333 (ν_4), 1275 (C–OH), 1101 (C–OM), 1034 (ν_2), 945 (ρ_ν), 837 (ν_3), 732 (ν_5), 671 (ρ_w), 563 (MO), 486 (MN), $\nu_1 - \nu_4 = 166$. UV–vis (λ_{max} nm, $\varepsilon \times 10^4 \text{ M}^{-1} \text{ cm}^{-1}$, DMF): 324, 3.66; 385, 3.29.

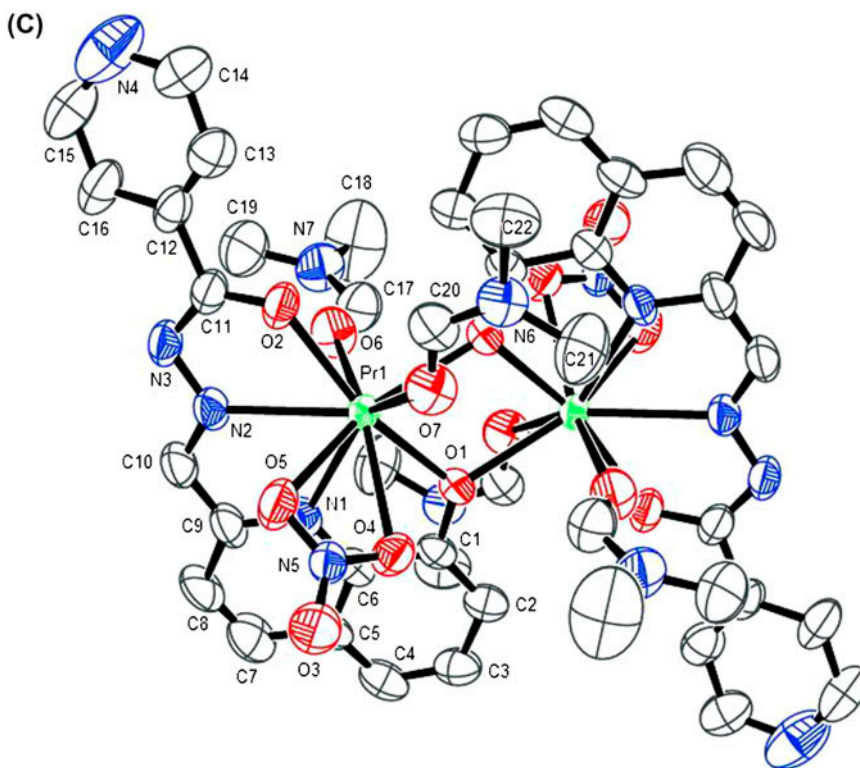


Figure 2. (Continued)

Complex **2c** was prepared from equimolar amounts of $\text{Pr}(\text{NO}_3)_3 \cdot 6\text{H}_2\text{O}$ with **1c** (0.0584 g, 0.2 mM) by the same way as **2a**. Yield: 0.096 g, 75.1%. IR (KBr) ($\nu_{\text{max}}/\text{cm}^{-1}$): 3443 (OH, H_2O), 1591 (C=N, azomethine), 1571 (C=N, pyridine), 1544 (C=N, pyridine), 1497 (ν_1), 1333 (ν_4), 1099 (C-OM), 1061 (ν_2), 902 (ρ_τ), 842 (ν_3), 734 (ν_5), 612 (ρ_w), 561 (MO), 487 (MN), $\nu_1 - \nu_4 = 164$. UV-vis (λ_{max} nm, $\epsilon \times 10^4 \text{ M}^{-1} \text{ cm}^{-1}$, DMF): 330, 4.16; 374, 3.29.

2.5. Determination of crystal structures

The orange transparent, X-ray quality crystals of **2a**, **2b**, and **2c** were obtained by vapor diffusion of diethyl ether into DMF solution of the metal complexes at room temperature for two weeks. The radiation used was graphite-monochromated Mo K α radiation (0.71073 Å) and the data were collected on a Bruker APEX area-detector diffractometer by the ω - 2θ scan technique at 298(2) or 296(2) K. The structures were solved by direct methods. All non-hydrogen atoms were refined anisotropically by full-matrix least-squares on F^2 . Primary non-hydrogen atoms were found from direct methods and secondary non-hydrogen atoms were found from difference maps. The hydrogens were added geometrically and their positions and thermal vibration factors were constrained. All calculations were performed using SHELXS-97 and SHELXL-97 [28]. Crystal data and structure refinements for the X-ray structural analyses are presented in table 1.

Table 1. Crystal data and structure refinement for the metal complexes.

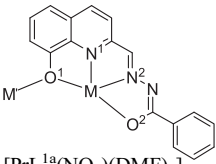
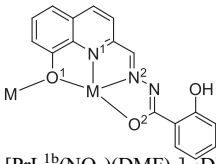
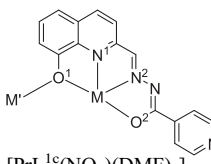
Complex	[PrL ^{1a} (NO ₃)(DMF) ₂] ₂	[PrL ^{1b} (NO ₃)(DMF) ₂] ₂ ·DMF	[PrL ^{1c} (NO ₃)(DMF) ₂] ₂
Chemical formula	C ₄₆ H ₅₀ N ₁₂ O ₁₄ Pr ₂	C ₄₉ H ₅₇ N ₁₃ O ₁₇ Pr ₂	C ₄₄ H ₄₈ N ₁₄ O ₁₄ Pr ₂
Formula weight	1276.80	1381.90	1278.78
<i>T</i> (K)	298(2)	298(2)	296(2)
Wavelength (Å)	0.71073	0.71073	0.71073
Radiation	Mo Kα	Mo Kα	Mo Kα
Crystal system	Monoclinic	Monoclinic	Triclinic
Space group	<i>P</i> 2 ₁ / <i>c</i>	<i>P</i> 2 ₁ / <i>c</i>	<i>P</i> 2 ₁ / <i>c</i>
<i>a</i> (Å)	11.1675(11)	25.222(2)	11.068(9)
<i>b</i> (Å)	18.6030(17)	17.7545(9)	18.550(15)
<i>c</i> (Å)	12.4937(12)	13.0656(7)	12.364(10)
α (°)	90.000	90.000	90.000
β (°)	93.6490(10)	94.5170(10)	94.091(14)
γ (°)	90.00	90.00	90.00
<i>V</i> (Å ³)	2590.3(4)	5832.5(6)	2532(3)
<i>Z</i>	2	4	2
<i>D</i> _c (g cm ⁻³)	1.637	1.574	1.677
μ (mm ⁻¹)	1.934	1.729	1.980
<i>F</i> (0 0 0)	1280	2784	1280
Crystal size (mm)	0.15 × 0.09 × 0.06	0.40 × 0.38 × 0.10	0.25 × 0.24 × 0.20
θ _{min} /max (°)	2.61–25.02	2.69–25.02	1.84–28.81
Index ranges	−11 ≤ <i>h</i> ≤ 13, −20 ≤ <i>k</i> ≤ 22, −13 ≤ <i>l</i> ≤ 14	−30 ≤ <i>h</i> ≤ 21, −19 ≤ <i>k</i> ≤ 21, −15 ≤ <i>l</i> ≤ 15	−14 ≤ <i>h</i> ≤ 10, −24 ≤ <i>k</i> ≤ 24, −15 ≤ <i>l</i> ≤ 16
Reflections collected	10,340	29,047	15,709
Independent reflections	4549 (<i>R</i> _{int} = 0.1198)	10,269 (<i>R</i> _{int} = 0.0689)	6387 (<i>R</i> _{int} = 0.0691)
Absorption correction	Semi-empirical from equivalents	Semi-empirical from equivalents	Semi-empirical from equivalents
Max. and min. transmission	0.8928 and 0.7602	0.8461 and 0.5447	0.6928 and 0.6374
Refinement method	Full-matrix least-squares on <i>F</i> ²	Full-matrix least-squares on <i>F</i> ²	Full-matrix least-squares on <i>F</i> ²
Data/restraints/parameters	4549/0/338	10,269/0/770	6387/0/339
Goodness-of-fit on <i>F</i> ²	1.101	1.038	1.015
Final <i>R</i> indices [<i>I</i> > 2σ(<i>I</i>)]	<i>R</i> ₁ = 0.0815, <i>wR</i> ₂ = 0.1393	<i>R</i> ₁ = 0.0502, <i>wR</i> ₂ = 0.0895	<i>R</i> ₁ = 0.0540, <i>wR</i> ₂ = 0.1398
<i>R</i> indices (all data)	<i>R</i> ₁ = 0.1714, <i>wR</i> ₂ = 0.1702	<i>R</i> ₁ = 0.1049, <i>wR</i> ₂ = 0.1161	<i>R</i> ₁ = 0.0883, <i>wR</i> ₂ = 0.1768
ρ _{min} /max (e Å ⁻³)	1.730/−1.728	1.228/−0.725	1.214/−2.026

3. Results and discussion

3.1. The crystal structure of complexes

Comparing IR bands between ligands and powder Pr^{III} complexes, phenolate oxygen, nitrogen of quinolinato unit, C=N azomethine group, O=C–NH– group of the aroylhydrazones side chain, and coordinated waters participate in the Pr^{III} complexes; bidentate nitrates participate in Pr^{III} complexes. All these Pr^{III} complexes are orange and stable in air, soluble in DMF and DMSO, slightly soluble in methanol, ethanol, acetonitrile, ethyl acetate, acetone, THF, and CHCl₃. The melting points of all the powder complexes exceed 300 °C. The molar conductivities Λ_M in DMF solution are 28.4, 46.1, and 42.2 cm² Ω⁻¹ M⁻¹ for **2a**, **2b**, and **2c**, respectively, indicating that they are non-electrolytes [29].

Table 2. Comparison of the structural parameters of **1a**, **1b**, and **1c** binding to Pr^{III} centers.

			
	[PrL ^{1a} (NO ₃)(DMF) ₂] ₂	[PrL ^{1b} (NO ₃)(DMF) ₂] ₂ ·DMF	[PrL ^{1c} (NO ₃)(DMF) ₂] ₂
M–O1	2.490(9)	2.488(5), 2.467(4)	2.441(4)
M–N1	2.556(11)	2.579(6), 2.584(6)	2.544(5)
M–N2	2.588(11)	2.627(6), 2.620(6)	2.577(5)
M–O2	2.375(9)	2.435(5), 2.425(4)	2.365(5)
M'–O1	2.437(8)	2.453(5), 2.468(4)	2.436(4)
O1–M–N1	63.0(3)	63.79(18), 64.19(17)	63.80(15)
N1–M–N2	61.2(4)	60.7(2), 60.77(19)	61.09(18)
N2–M–O2	60.9(4)	60.69(19), 60.65(18)	60.21(18)
Distance between M···M'	4.0698(16)	4.0960(9), 4.0843(8)	4.051(2)

3.1.1. The crystal structure of 2a. Figure 2(A) shows the structure of [PrL^{1a}(NO₃)(DMF)₂]₂ for **2a**. **1a** is a dibasic tetradentate ligand, binding to Pr^{III} through phenolate oxygen, nitrogen of quinolinato unit, the C=N group, and [−]O–C=N– enolized and deprotonated from O=C–NH– of the benzoylhydrazone side chain. One DMF binds orthogonally to the ligand plane from one side to the metal ion, while another DMF and a bidentate nitrate bind from the other side. Dimerization of this monomeric unit occurs through the phenolate oxygens leading to a central planar four-membered (PrO)₂ ring with a Pr···Pr separation of 4.0698(16) Å as shown in table 2. At the dimerization site, a 2 Å offset of the two parallel “PrL^{1a}-planes” takes place. The center of symmetry according to the crystallographic coordinates is located in the middle of the four-membered (PrO)₂ ring formed by the two Pr ions and the phenolic oxygens. This nine-coordinate structure of a binuclear complex with a 1:1 metal-to-ligand stoichiometry is similar to that of [YL(NO₃)

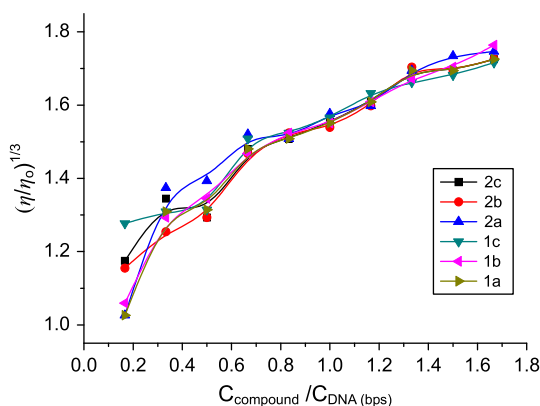


Figure 3. Effects of increasing amounts of the investigated compounds on the relative viscosity of CT-DNA in 5 mM Tris–HCl buffer solution (pH 7.20) containing 50 mM NaCl at 25.00 ± 0.01 °C. The concentration of CT-DNA was 50 μM (bps).

(DMF)₂]₂Cl₂·2(DMF) or [LaL(NO₃)(MeOH)₂]₂(NO₃)₂, where L-H is 2-[(8-hydroxyquinolinyl)methylene]hydrazinecarboxamide and is tetradentate to yttrium(III) or lanthanum(III) through the phenolate oxygen, nitrogen of quinolinato unit, the C=N and C=O of the semicarbazone side chain [5]. However, there are some marked differences between them. Importantly, O=C–NH– group of the benzoylhydrazone side chain has enolized and deprotonated into [−]O–C=N– group after the formation of [PrL^{1a}(NO₃)(DMF)₂]₂, where the C–O– band length is 1.279(14) Å and the N=C double band length is 1.353(17) Å (The normal band lengths of C=O, C–N, C–O and C=N are 1.19–1.23, 1.47–1.50, 1.30–1.39 and 1.34–1.38 Å, respectively [30]). Carbonyl groups of the semicarbazone side chains have not enolized in [YL(NO₃)(DMF)₂]₂Cl₂·2(DMF) and [LaL(NO₃)(MeOH)₂]₂(NO₃)₂. The deprotonation and enolization may arise from triethylamine added to the reaction mixtures to deprotonate the phenolic hydroxyl substituent of 8-hydroxyquinolate during formation of the Pr^{III} complex. As a result, [PrL^{1a}(NO₃)(DMF)₂]₂ is neutral and non-electrolyte as proved by the values of molar conductivity in DMF solution, while both [YL(NO₃)(DMF)₂]₂Cl₂·2(DMF) and [LaL(NO₃)(MeOH)₂]₂(NO₃)₂ are electrolytes.

3.1.2. The crystal structure of 2b. The structure of [PrL^{1b}(NO₃)(DMF)₂]₂·DMF for **2b** with a 1:1 metal-to-ligand stoichiometry and nine-coordination is shown in figure 2(B), which indicates that there are two same molecules and a free DMF in the crystal unit cell. Similarly to **1a**, ligand **1b** is dibasic tetradentate, binding to Pr^{III} through the phenolate oxygen, nitrogen of quinolate and the C=N group (methylene), [−]O–C=N– group enolized and deprotonated from O=C–NH– of the 2'-hydroxybenzoylhydrazone side chain, in which the [−]O–C and N=C band lengths are 1.262(9) and 1.331(10) Å for Pr(1) molecule, and 1.275(8) and 1.321(9) Å for Pr(2) molecule, respectively. Also, one DMF binds orthogonally to the ligand plane from one side to the metal ion, while another DMF and a bidentate nitrate bind from the other side. Dimerization of the monomeric unit occurs through phenolate oxygens leading to a central four-membered (PrO)₂ ring with Pr(1)⋯Pr(1) separation of 4.0960(9) Å in one molecule and Pr(2)⋯Pr(2) separation of 4.0843(8) Å in another. At the dimerization site, a 2 Å offset of the two parallel “PrL^{1b}-planes” takes place. The center of symmetry is located in the middle of the four-membered (PrO)₂ ring formed by two Pr ions and the phenolic oxygens. The 2'-hydroxyl substituent linked with benzoylhydrazone does not take part in binding to Pr^{III}, largely due to the long distance (5.990 Å) between the substituent and Pr^{III}, but it may be involved in an intramolecular hydrogen band with the adjacent nitrogen, forming a stabilized six-membered ring. A DMF is not coordinated in Pr(2) complex, indicating that this DMF has two roles when binding to Pr^{III}.

3.1.3. The crystal structure of 2c. Figure 2(C) shows the structure of [PrL^{1c}(NO₃)(DMF)₂]₂. This nine-coordinate structure with a 1:1 metal-to-ligand stoichiometry is similar to those of **2a** and **2b**. **1c** also is a dibasic tetradentate ligand, binding to Pr^{III} through the phenolate oxygen, nitrogen of quinolate, the C=N (methylene), and [−]O–C=N– enolized and deprotonated from O=C–NH– of the isonicotinylhydrazone side chain with [−]O–C and N=C band lengths of 1.254(8) and 1.306(10) Å. One DMF binds orthogonally to the ligand plane from one side to the metal ion, while another DMF and a bidentate nitrate bind from the other side. Dimerization of this monomeric unit also occurs through the phenolate oxygens leading to a central four-membered (PrO)₂ ring with a Pr⋯Pr separation of 4.051

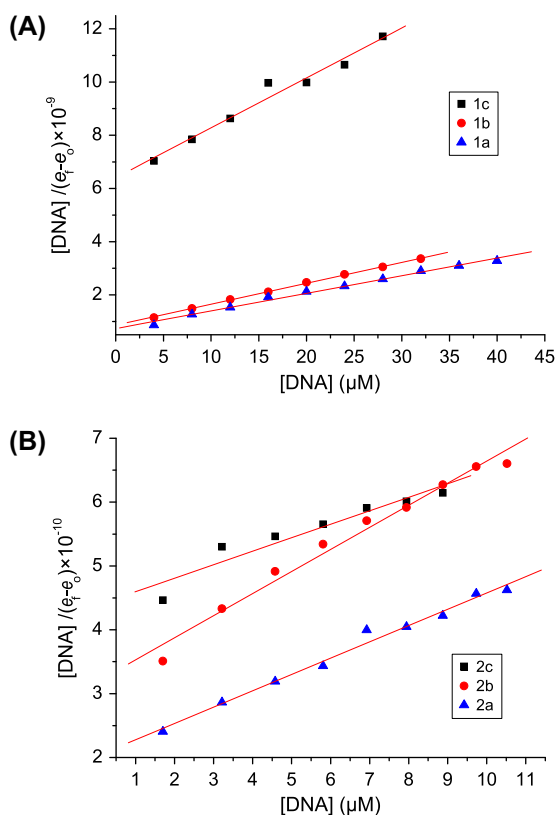


Figure 4. Plots of $[\text{DNA}]/(\epsilon_f - \epsilon_a)$ vs. $[\text{DNA}]$ for ligands (A) and Pr^{III} complexes (B).

Table 3. K_b , K_{SV} , and FC_{50} for ligands and Pr^{III} complexes.

Compound	$K_b \times 10^5 \text{ M}^{-1}$	$K_{\text{SV}} \times 10^4 \text{ M}^{-1}$	FC_{50} (μM) ($C_{\text{compound}}/C_{\text{DNA}}$, nucleotides)
1a	0.9032 ± 0.0444	2.086 ± 0.014	48.18 (12.05 : 1)
1b	0.9142 ± 0.0495	2.352 ± 0.018	38.95 (9.738 : 1)
1c	0.2767 ± 0.0559	1.405 ± 0.013	66.30 (16.58 : 1)
2a	1.262 ± 0.139	9.245 ± 0.551	16.46 (4.115 : 1)
2b	1.085 ± 0.139	5.684 ± 0.420	24.90 (6.226 : 1)
2c	0.9381 ± 0.0591	3.166 ± 0.366	31.36 (7.841 : 1)

(2) Å. At the dimerization site, a 2 Å offset of the two parallel “PrL^{1c}-planes” takes place. The center of symmetry is located in the middle of the four-membered (PrO)₂ ring formed by the two Pr atoms and the phenolic oxygens.

However, the three crystal structures are similar to each other and similar to other lanthanide complexes derived from 8-hydroxyquinoline-2-carboxaldehyde and aroylhydrazones as reported [12–19]. All these complexes are non-electrolytes. Lanthanide ions and structurally similar Schiff bases can form a series of structurally similar binuclear and 1 : 1 metal-to-ligand complexes by nine-coordination at Ln^{III} with geometry of distorted edge-sharing mono-capped square-antiprism of $[\text{LnL}(\text{NO}_3)(\text{DMF})_2]_2$ (Ln = La³⁺, Nd³⁺, Sm³⁺, Eu³⁺,

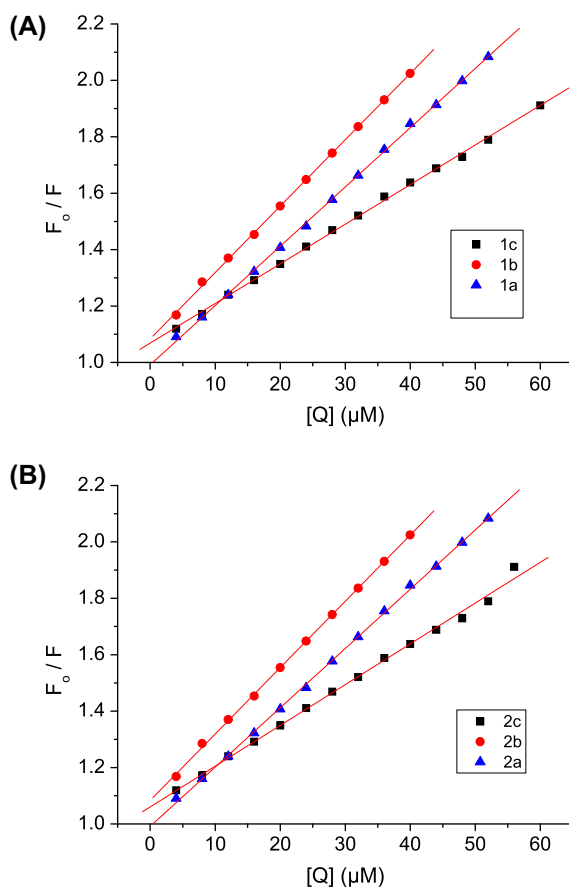


Figure 5. The Stern–Volmer plots for ligands (A) and Pr^{III} complexes (B) in EB-DNA systems. $\lambda_{\text{ex}} = 525$ nm, $\lambda_{\text{em}} = 587$ nm, 298 K. The concentration of DNA is 4.0 μM (nucleotides) and the concentration of EB is 0.32 μM .

Tb³⁺, Dy³⁺, Ho³⁺, and Er³⁺) except for Yb^{III} which has eight-coordination with geometry of distorted edge-sharing dodecahedron for [YbL(NO₃)(DMF)]₂. This difference may be due to the small size of Yb^{III}.

3.2. DNA-binding properties

3.2.1. Viscosity titration measurements. Viscosity titration measurements were carried out to clarify the interaction modes between the investigated compounds and CT-DNA. Hydrodynamic measurements that are sensitive to length change of DNA (i.e. viscosity and sedimentation) are regarded as the least ambiguous and the most critical criteria for binding modes in solution in absence of crystallographic structural data, as viscosity is proportional to L^3 for rod-like DNA of length L [23, 31]. Intercalation involves the insertion of a planar molecule between DNA base pairs, resulting in a decrease in the DNA helical twist and lengthening of the DNA; therefore, intercalators cause the unwinding and lengthening of

DNA helix as base pairs become separated to accommodate the binding compound [32]. Agents bound to DNA through groove binding do not alter the relative viscosity of DNA, and agents bound to DNA through electrostatic binding will bend or kink the DNA helix, reducing its effective length and its viscosity, concomitantly [33, 34]. With the ratio of the investigated compound to DNA (bps) increasing, the relative viscosity of DNA increases steadily as shown in figure 3, indicating that intercalation takes place between the compounds with DNA helix, though there are not significant differences between ligands and complexes.

3.2.2. UV-vis spectroscopic study. The UV-vis absorption spectra of the investigated compounds in the absence and in the presence of CT-DNA were obtained in DMF: Tris-HCl buffer (5 mM, pH 7.20) containing 50 mM NaCl of 1 : 100 solutions, respectively. The UV-vis spectra of ligands have two types of absorption bands of λ_{\max} at 295 nm ($\epsilon = 3.55 \times 10^4 \text{ M}^{-1} \text{ cm}^{-1}$) and 323 nm ($\epsilon = 2.11 \times 10^4 \text{ M}^{-1} \text{ cm}^{-1}$), 294 nm ($\epsilon = 3.16 \times 10^4 \text{ M}^{-1} \text{ cm}^{-1}$) and 329 nm ($\epsilon = 2.36 \times 10^4 \text{ M}^{-1} \text{ cm}^{-1}$), and 290 nm ($\epsilon = 2.86 \times 10^4 \text{ M}^{-1} \text{ cm}^{-1}$) and 325 nm ($\epsilon = 1.78 \times 10^4 \text{ M}^{-1} \text{ cm}^{-1}$), respectively, for **1a**, **1b**, and **1c**, while the UV-vis spectra of Pr^{III} complexes have two typical bands of λ_{\max} at 321 nm ($\epsilon = 4.83 \times 10^4 \text{ M}^{-1} \text{ cm}^{-1}$) and 368 nm ($\epsilon = 2.76 \times 10^4 \text{ M}^{-1} \text{ cm}^{-1}$), 324 nm ($\epsilon = 3.66 \times 10^4 \text{ M}^{-1} \text{ cm}^{-1}$) and 385 nm ($\epsilon = 3.29 \times 10^4 \text{ M}^{-1} \text{ cm}^{-1}$), and 330 nm ($\epsilon = 4.16 \times 10^4 \text{ M}^{-1} \text{ cm}^{-1}$) and 374 nm ($\epsilon = 3.29 \times 10^4 \text{ M}^{-1} \text{ cm}^{-1}$), respectively, for **2a**, **2b**, and **2c**, which can be assigned to π - π^* transition of aromatic rings, π - π^* of conjugated aromatic rings, and the charge transfer from ligand-to-metal ions ($\text{L} \rightarrow \text{Pr}^{3+}$), respectively [35, 36]. Upon successive addition of CT-DNA (bps), the UV-vis absorption bands of **1a**, **1b**, and **1c** show a progressive hypochromism of 34.3% at 295 nm, 30.1% at 294 nm, and 8.4% at 290 nm by approximately saturated titration end points at $C_{\text{DNA}} : C_{\text{ligand}} = 1.4$ – $2.2 : 1$, respectively, with 1, 3, and 0 nm red shifts of absorption bands. Ligands **1a**, **1b**, and **1c** show progressive hypochromism of 11.1% at 323 nm, 18.1% at 329 nm, and 1.0% at 325 nm, respectively, with 1, 3, and 0 nm blue shifts. Similarly, upon successive additions of CT-DNA (bps), the UV-vis absorption bands of **2a**, **2b**, and **2c** show progressive hypochromism of 47.1% at 321 nm, 43.5% at 324 nm, and 40.6% at 330 nm by approximately saturated titration end points at $C_{\text{DNA}} : C_{\text{complex}} = 1.5 : 1$, respectively, with 0, 0, and 2 red shifts of absorption bands. Complexes **2a**, **2b**, and **2c** show progressive hypochromism of 50.9% at 368 nm, 45.3% at 385 nm, and 46.2% at 374 nm, respectively, with 2, 3, and 0 nm blue shifts. The obvious hypochromisms further indicate the strong stacking interaction between the aromatic chromophore of the compound and base pairs of DNA rather than non-covalent intercalative binding of compound to DNA helix [37, 38]. The magnitude of hypochromism is parallel to the intercalative strength and the affinity of a compound binding to DNA [31]. Figure 4(A) and (B) shows plots of $[\text{DNA}]/(\epsilon_{\text{f}} - \epsilon_{\text{a}})$ versus $[\text{DNA}]$ for ligands and complexes, respectively. The binding constants ($K_{\text{b}} = 0.2767$ – $0.9142 \times 10^5 \text{ M}^{-1}$ for ligands, $K_{\text{b}} = 0.9381$ – $1.262 \times 10^5 \text{ M}^{-1}$ for Pr^{III} complexes) of DNA were determined (listed in table 3). Compared with EB (classical intercalative agent) binding to DNA ($K_{\text{b}} = 0.3068 \times 10^5 \text{ M}^{-1}$) investigated at the same conditions [20], these Pr^{III} complexes present higher binding abilities to DNA than either ligands or EB. There is no significant difference in binding to DNA between these Pr^{III} complexes and those derived from 3-carbaldehyde chromone with isonicotinyl hydrazine, 1-phenyl-3-methyl-4-formyl-2-pyrazolin-5-one (PMFP) with isonicotinyl hydrazine, and PMFP with 4-aminophenazone, in which $\text{Ln} = \text{La}^{3+}$, Nd^{3+} , Sm^{3+} , Tb^{3+} , Dy^{3+} , and Yb^{3+} and $K_{\text{b}} = 2.44$ – $7.6 \times 10^5 \text{ M}^{-1}$

[39–41]. However, these Pr^{III} complexes show slightly weaker binding to DNA than those derived from lanthanide metal ions with 8-hydroxyquinoline-7-carbaldehyde-(isonicotinyl) hydrazone ($K_b = 9.5\text{--}16.7 \times 10^5 \text{ M}^{-1}$) and 8-hydroxyquinoline-7-carbaldehyde-(benzoyl) hydrazone ($K_b = 2.938\text{--}26.13 \times 10^5 \text{ M}^{-1}$) [20, 21]. Moreover, they show weaker binding to CT-DNA than Sm(III) complex derived from Congo red (CR) binding to herring sperm DNA, in which the K_b of Sm(III)(CR)₃ complex is $6.25 \times 10^6 \text{ M}^{-1}$ at 18 °C and $1.11 \times 10^7 \text{ M}^{-1}$ at 26 °C [42].

3.2.3. DNA-EB quenching assay. The fluorescence emission intensity of DNA-EB system decreased dramatically upon increasing amounts of either ligands or Pr^{III} complexes. Stern–Volmer plots are shown in figure 5 and the data of Stern–Volmer quenching constants are collected in table 1. The values of K_{SV} are $1.405\text{--}9.245 \times 10^4 \text{ M}^{-1}$ for ligand and Pr^{III} complexes and the loss of fluorescence intensity at the maximum wavelength indicates that most of the EB molecules have been displaced from EB-DNA complex by the quencher at the approximately saturated end point, which indicates further that the intercalative binding takes place between the investigated compound and DNA. Stern–Volmer quenching constant can also be interpreted as the association or binding constant of the complexation reaction [43]. Compared with the values of K_{SV} of other lanthanide complexes derived from 8-hydroxyquinoline-2(7)-carboxaldehyde with aroylhydrazines, these Pr^{III} complexes present middle levels of binding to DNA [12–19]. DNA intercalators have been used extensively as antitumor, antineoplastic, antimalarial, antibiotic, and antifungal agents [31]. There is a criterion for screening antitumor drugs from others by DNA-EB fluorescent tracer method, i.e. a compound may be used as a potential antitumor drug if it causes a 50% loss of DNA-EB fluorescence intensity by fluorescent titration before the molar concentration ratio of the compound to DNA (nucleotides) does not overrun 100 : 1 [44]. FC_{50} value is introduced to denote the molar concentration of a compound that causes a 50% loss in the fluorescence intensity of the EB-DNA system. According to the data of FC_{50} and the molar ratios of compounds to DNA as shown in table 3, at FC_{50} , all the molar concentration ratios of the investigated compounds to DNA (4.115–16.58 : 1) are significantly under 100 : 1, indicating that all these investigated compounds are probably used as potential antitumor drugs and the antitumor activities of Pr^{III} complexes may be better than that of ligands. However, their pharmacodynamical, pharmacological and toxicological properties should be further studied *in vivo*.

4. Conclusion

Pr^{III} and three synthesized ligands form binuclear Pr^{III} complexes with 1 : 1 metal-to-ligand stoichiometry and nine-coordinate Pr^{III} indicated by X-ray crystal structural analyses. Ligands are dibasic tetradentates, binding to Pr^{III} through the phenolate oxygen, nitrogen of quinolate, the C=N of methylene, and $\text{O}^-\text{C}=\text{N}-$ enolized and deprotonated from $\text{O}=\text{C}-\text{NH}-$ of the aroylhydrazone side chain. Dimerization of the monomeric unit occurs through the phenolate oxygens leading to a planar four-membered (PrO)₂ ring. These crystal structures are similar to each other and to other nine-coordinate lanthanide complexes with geometry of distorted edge-sharing mono-capped square-antiprism of $[\text{LnL}(\text{NO}_3)(\text{DMF})_2]_2$ ($\text{Ln} = \text{La}^{\text{III}}, \text{Nd}^{\text{III}}, \text{Sm}^{\text{III}}, \text{Eu}^{\text{III}}, \text{Tb}^{\text{III}}, \text{Dy}^{\text{III}}, \text{Ho}^{\text{III}}, \text{Er}^{\text{III}}$) except for

eight-coordinate Yb^{III} with distorted edge-sharing dodecahedron of [YbL(NO₃)(DMF)]₂, derived from 8-hydroxyquinoline-2-carboxaldehyde and aroylhydrazines. The ligands and Pr^{III} complexes can bind to CT-DNA through intercalation with the binding constants of 10⁵ M⁻¹. Compared with other lanthanide complexes derived from 8-hydroxyquinoline-2(7)-carboxaldehyde with aroylhydrazines, these Pr^{III} complexes present middle levels or slight weaker binding to DNA, even weaker binding to CT-DNA than Sm(III) complex derived from CR binding to herring sperm DNA. However, they may be useful as potential antitumor drugs. Future research efforts will focus on achieving their biological and other properties.

Supplementary material

CIF files for the X-ray crystal structures have been deposited with the Cambridge Crystallographic Data Center (CCDC 993157, 993160 and 993159). Copies of this information may be obtained free of charge from the Director, CCDC, 12 Union Road, Cambridge, CB2 1EZ, UK (Fax: +44 1223 336033; E-mail: deposit@ccdc.cam.ac.uk or <http://www.ccdc.cam.ac.uk>). Supplementary materials associated with this article can be found in the online version.

Acknowledgements

The study was supported by Gansu Key Subject of Applied Chemistry (GSACKS20130113) and Longdong University Doctor Fund.

References

- [1] S. Mahadevan, M. Palaniandavar. *Inorg. Chim. Acta*, **254**, 291 (1997).
- [2] S.J. Lippard. *Acc. Chem. Res.*, **11**, 211 (1978).
- [3] S.M. Hecht. *Acc. Chem. Res.*, **19**, 383 (1986).
- [4] D. Parker, R.S. Dickens, H. Puschmann, C. Crossland, J.A.K. Howard. *Chem. Rev.*, **102**, 1977 (2002).
- [5] M. Albrecht, O. Osetska, R. Fröhlich. *Dalton Trans.*, **23**, 3757 (2005).
- [6] R.B. Hunter, W. Walker. *Nature*, **178**, 47 (1956).
- [7] D.M. Kramsch, A.J. Aspen, L.J. Rozler. *Science*, **213**, 1511 (1981).
- [8] E.M. Eudnett, P.D. Mooney. *J. Med. Chem.*, **13**, 786 (1970).
- [9] E.M. Eudnett, W.J. Dunn. *J. Med. Chem.*, **15**, 339 (1972).
- [10] L.H. Schmidt. *Ann. Rev. Microbiol.*, **23**, 427 (1969).
- [11] A.A. El-Asmy, A.Z. El-Sonbati, A.A. Ba-Issa, M. Mounir. *Transition Met. Chem.*, **15**, 222 (1990).
- [12] Y.C. Liu, Z.Y. Yang. *BioMetals*, **22**, 733 (2009).
- [13] Y.C. Liu, Z.Y. Yang. *J. Org. Chem.*, **694**, 3091 (2009).
- [14] Y.C. Liu, Z.Y. Yang. *J. Inorg. Biochem.*, **103**, 1014 (2009).
- [15] Y.C. Liu, Z.Y. Yang. *Inorg. Chem. Commun.*, **12**, 704 (2009).
- [16] Y.C. Liu, Z.Y. Yang. *Eur. J. Med. Chem.*, **44**, 5080 (2009).
- [17] Y.C. Liu, X.H. Jiang, Z.Y. Yang, X.D. Zheng, J.N. Liu, T.L. Zhou. *Appl. Spectrosc.*, **64**, 980 (2010).
- [18] Y.C. Liu, Z.Y. Yang. *J. Biochem.*, **147**, 381 (2010).
- [19] Y.C. Liu, Z.Y. Yang, K.J. Zhang, Y. Wu, J.H. Zhu, T.L. Zhou. *Aust. J. Chem.*, **64**, 345 (2011).
- [20] Y.C. Liu, K.J. Zhang, R.X. Lei, J.N. Liu, T.L. Zhou, Z.Y. Yang. *J. Coord. Chem.*, **65**, 2041 (2012).
- [21] Y.C. Liu, K.J. Zhang, Y. Wu, J.Y. Zhao, J.N. Liu, T.L. Zhou. *Chem. Biodivers.*, **9**, 1533 (2012).
- [22] F. Zsila, Z. Bikádi, M. Simonyi. *Org. Biomol. Chem.*, **2**, 2902 (2004).
- [23] D. Suh, J.B. Chaires. *Bioorg. Med. Chem.*, **3**, 723 (1995).
- [24] S. Satyanarayana, J.C. Dabrowiak, J.B. Chaires. *Biochemistry*, **31**, 9319 (1992).

- [25] A. Wolfe, G.H. Shimer Jr, T. Meehan. *Biochemistry*, **26**, 6392 (1987).
- [26] P.X. Xi, Z.H. Xu, X.H. Liu, F.J. Cheng, Z.Z. Zeng. *Spectrochim. Acta, Part A*, **71**, 523 (2008).
- [27] A. Ayar, B. Mercimek. *Process Biochem.*, **41**, 1553 (2006).
- [28] G.M. Sheldrick. *Acta Crystallogr. A*, **46**, 467 (1990).
- [29] W.J. Geary. *Coord. Chem. Rev.*, **7**, 81 (1971).
- [30] X.M. Chen, J.W. Cai. *Single-crystal Structural Analysis. Principles and Practices*, Science Press, Beijing (2003).
- [31] D.S. Sigman, A. Mazumder, D.M. Perrin. *Chem. Rev.*, **93**, 2295 (1993).
- [32] R. Palchoudhuri, P.J. Hergenrother. *Curr. Opin. Biotechnol.*, **18**, 497 (2007).
- [33] B.D. Wang, Z.Y. Yang, P. Crewdson, D.Q. Wang. *J. Inorg. Biochem.*, **101**, 1492 (2007).
- [34] S. Satyanarayana, J.C. Dabrowiak, J.B. Chaires. *Biochemistry*, **31**, 9319 (1992).
- [35] T.M.A. Ismail. *J. Coord. Chem.*, **58**, 141 (2005).
- [36] M.M. Moawad, W.G. Hanna. *J. Coord. Chem.*, **55**, 439 (2002).
- [37] J.K. Barton, A.T. Danishefsky, J.M. Goldberg. *J. Am. Chem. Soc.*, **106**, 2172 (1984).
- [38] H.L. Lu, J.J. Liang, Z.Z. Zeng, P.X. Xi, X.H. Liu, F.J. Chen, Z.H. Xu. *Transition Met. Chem.*, **32**, 564 (2007).
- [39] Y. Li, Z.Y. Yang. *J. Coord. Chem.*, **63**, 1960 (2010).
- [40] M.F. Wang, Z.Y. Yang, Y. Li, H.G. Li. *J. Coord. Chem.*, **64**, 2974 (2011).
- [41] M.F. Wang, Z.Y. Yang, Z.C. Liu, Y. Li, T.R. Li, M.H. Yan, X.Y. Cheng. *J. Coord. Chem.*, **65**, 3805 (2012).
- [42] H.Z. Pan, X.M. Wang, H.B. Li, Q. Yang, L.S. Ding. *J. Coord. Chem.*, **63**, 4347 (2010).
- [43] L.A. Bagatolli, S.C. Kivatinitz, G.D. Fidelio. *J. Pharm. Sci.*, **85**, 1131 (1996).
- [44] Z.L. Li, J.H. Chen, K.C. Zhang, M.L. Li, R.Q. Yu. *Sci. China Ser. B*, **21**, 1193 (1991).